THE OCEAN-SEDIMENT SYSTEM AND STRATIGRAPHIC MODELING IN LARGE BASINS

BERND J. HAUPT
Sonderforschungsbereich 313, Universität Kiel, Heinrich-Hecht-Platz 10, D-24118 Kiel, Germany
AND
KARL STATTEGGER
Geologisch-Paläontologisches Institut, Universität Kiel, Olshausenstraβe 40-60, D-24118 Kiel, Germany

ABSTRACT: The new three-dimensional sedimentation model SEDLOB (SEDimentation in Large Ocean Basins) is used to simulate the climatically driven Quaternary sedimentation history of the northern North Atlantic. The forward model SEDLOB is driven by the thermohaline oceanic circulation and coupled to an ocean general-circulation model. Glacial and interglacial periods produce distinct basinwide sediment accumulation patterns that are strongly influenced by the prescribed sediment input and its physical properties. Taking into account the stratigraphic succession of glacial and interglacial time periods measured in sediment cores with high precision, it is possible to stack the typical sedimentation patterns to a climatically induced sediment fill of an ocean basin. Examples with maps and synthetic cross sections are presented for the northern North Atlantic using stratigraphic data from sediment cores covering the last 2.62 m.y.

INTRODUCTION

Sedimentation processes, including erosion, transport, and deposition in large ocean basins, depend strongly on sediment input from various sources and on ocean circulation patterns. Sedimentation and ocean thermohaline circulation are controlled to a large extent by the morphology of a basin and by climate, and are subject to long-term tectonic and short-term climatic changes. Given a specific steady-state oceanic circulation pattern with its temperature, salinity, velocity fields, and convection depths, it is possible to add sediment defined by physical properties from various sources to the circulating water volumes. Process-oriented three-dimensional (3-D) modeling of sedimentation in large basins should be performed on the basis of (1) an adequate geologic/oceanographic database, (2) efficient algorithms and parameterization for the simulation of sedimentation processes, (3) accurate model initialization with respect to the external forcing of sedimentation, and (4) reproducible model validation compared to the modern state of the investigated system. Several forward models designed for specific sedimentary environments are driven by continuity equations defined from first principles (e.g., Ericksen et al., 1989; Tetzlaff and Harbaugh, 1989; Syvitski and Daughney, 1992; Cao and Lerche, 1994; Slingerland et al., 1994).

With respect to stratigraphic experiments, a numerical model should allow simulation of sediment distribution patterns on the sea floor, especially accumulation and erosion of sediments integrated over time intervals long enough to represent the stratigraphic architecture. Based on the stratigraphic record, this architecture is composed of succeeding sequences in a chronostratigraphic time frame.

Stratigraphic modeling involves simulating the geometry and the buildup of sediment sequences incorporating sequence stratigraphic concepts. Sedimentation processes are linked to basin subsidence and often expressed by the diffusion equation (e.g., Jervey, 1991; Kaufman et. al., 1991; Paola et al., 1992; Rivenaes, 1992; Flemings and Grotzinger, 1996). Stratigraphic models generate depositional sequences in a broad range of stratal geometries from a single diffusion equation with variations in initial and boundary conditions. The disadvantage lies in the very rough approximation of sediment transport.

In this paper we use the 3-D forward sedimentation model SEDLOB (SEDimentation in Large Ocean Basins) (Haupt et al., 1994, 1997; Haupt and Stattegger, 1996; Seidov and Haupt, 1997) to generate basinwide glacial and interglacial sedimentation patterns of the northern North Atlantic. Sediment accumulation is integrated over time spans covering succeeding cold and warm periods as defined by the high-resolution Pliocene–Pleistocene sedimentary record (cf. Tiedemann et al., 1994; Mudelsee, 1995). Synthetic stratigraphic sections are obtained from this climatically forced basin fill.

NUMERICAL MODELS

We combine an ocean general-circulation model (OGCM) of the northern North Atlantic with a three-dimensional model of sediment transport based on the output from the OGCM. This approach was first suggested by Haupt (1995) and Haupt et al. (1994, 1995). In this paper, we present the results of the sedimentation processes in the northern North Atlantic obtained using this combination modeling approach.

The results are based on the model runs with a $0.5° \times 0.5°$ horizontal resolution (95 grid points in both horizontal directions) and a high vertical resolution with 17 layers. From top to bottom the layer thicknesses are 50, 50, 50, 50, 100, 100, 100, 250, 250, 250, 250, 500, 500, 500, 500, 500, and 1000 m. The topography is taken from the ETOPO5 (1986) data set. This high vertical resolution is essential for calculating the sediment transport through gateways and cross sections; e.g., the Denmark Strait, the Iceland-Faeroe-Scotland-Ridge, or Barents Sea inflow and outflow.

In addition, we use a spherical coordinate system in which the equator is rotated up to 60°N along the zero meridian to minimize the convergence of meridians at high latitudes (Haupt et al., 1994, 1995). By this rotation we arrive at an almost equally spaced grid with approximately 55 km in both horizontal directions. Inside the rotated coordinate system, the coriolis force depends both on latitude, as in a normal nonrotated coordinate system, and on longitude.

OGCM

In this study we used the SCINNA model (Sensitivity and CIrculation in the Northern North Atlantic) (Haupt et al., 1994, 1995;

Numerical Experiments in Stratigraphy: Recent Advances in Stratigraphic and Sedimentologic Computer Simulations, SEPM Special Publications No. 62,

Schäfer-Neth, 1994), which is a three-dimensional fully prognostic OGCM, a modified version of the modular ocean model (Pacanowski et al., 1991). The SCINNA model is based on the primitive equation with conservation of mass, momentum, heat, and salt. At the surface, the model is forced by relaxation to prescribed sea surface temperatures and salinities, and by the momentum flux proportional to the wind stress.

Sedimentation Model

SEDLOB is a 3-D large-scale dynamic sedimentation model designed by Haupt (1995) and tested in Haupt et al. (1994, 1995). We emphasize that SEDLOB can be coupled to any 3-D OGCM that provides adequate input fields of temperature, salinity, velocity, and convection depth. The importance of convection depth input has been shown by Seidov and Haupt (1997). The model itself basically consists of two linked components: (1) a 3-D sediment transport model in the ocean interior and (2) a 2-D sediment transport model in a thin near-bottom layer following smoothed bottom topography (Figure 1). The lower two-dimensional (2-D) submodel, which uses the same horizontal resolution as the 3-D sediment transport model, is initialized and forced at every time step by the data generated within the 3-D submodel. The OGCM temperature, salinity, and velocity fields are projected on the smoothed bottom. In addition, near-bottom velocities are reduced to take bottom friction into account (Miller et al., 1977; Zanke, 1978; Sündermann and Klöcker, 1983). The sediment is continuously exchanged between both parts of SEDLOB depending on sediment concentration, vertical velocity, and settling velocity.

The 3-D sediment transport model calculates sediment transport in the water column. The transport equation is expanded by an additional term to compute the settling of sediment in the 3-D water column (Haupt et al., 1997); furthermore, SEDLOB simulates the lateral inflow and outflow of sediment from coastal sources such as rivers, the input of eolian dust, and ice-rafted debris from melting icebergs. Additionally, various biological factors, such as dying plankton and fecal pellets, can be included as parameterized sediment sources.

The coupled 2-D sediment transport model considers erosion, transport (sliding, rolling, and skipping), and deposition of sediments in a 1-cm-thick bottom layer following the bottom topography. The sediment content depends on the critical velocities for bed load, the suspended-load transport, and the actual sediment content within this layer. Deposition takes place in cases of reduced velocity, a rising bottom topography, or if the saturation point is reached. The saturation point describes the maximum possible sediment transport and is velocity dependent; however, sediment is eroded until the saturation point is reached, if the velocity increases, if the bottom topography descends, or if the water within this 2-D bottom layer is undersaturated. In all other cases, the available sediment is transported in this 2-D "rubber mat" (Figure 1), whereas the spatial differential settling velocity and the critical velocities for bed load and suspension load are checked at every time step. The relationship between the critical velocities and sediment transport is summarized in Figure 2. For the settling velocity, for the critical velocities initiating the bed load, for suspension-load transport, and for the corresponding equations for the transport itself we use polynomial equations [see review in Haupt (1995) and Haupt et al. (1997)]. We modified all of these equations to include the effects of the bottom slope; however, this effect of increasing or decreasing bottom slope inclination in the sediment transport direction is not a primary effect, and the polynomial equations depend mainly on grain size and form factor; temperature, salinity, density, and viscosity of sediment and sea water; and gravitational acceleration. The critical velocities for beginning of bed-load and suspension-load transport are shown in Figure 3. A detailed description of the model and

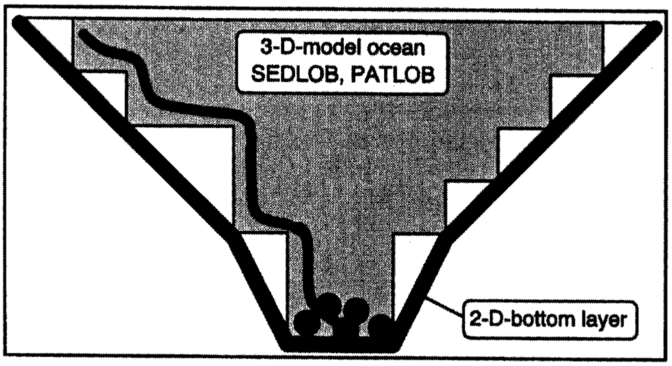

FIG. 1.—Coupling of the two submodels.

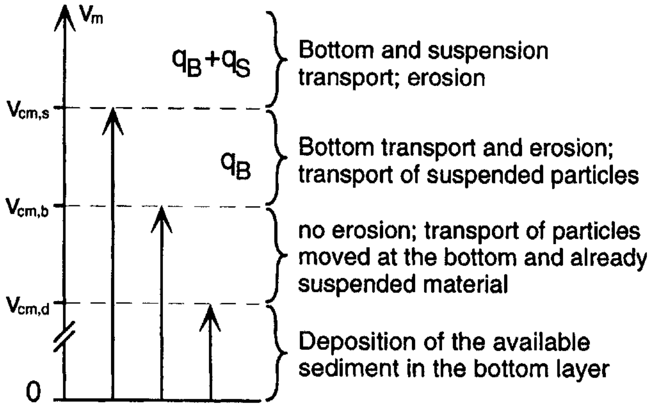

FIG. 2.—Critical velocities for initiating bed-load transport and suspension-load transport (see Figure 3). The formula for calculating the bed load transport is

$$q_B = \frac{1}{p} 10^{-7} \left(\frac{v_s^2 - v_{c,b}^2}{w_s^2} D*^2 \right)^2 v$$

where

$$D* = \left(\frac{\rho' g}{v^2} \right)^{1/3} d$$

and $p \approx 0.7$, and the formula for calculating the suspension transport is

$$q_s = 10^{-8} \frac{H}{h_1} \frac{\left(v_s^2 - v_{c,b}^2\right)\left(v_s^2 - v_{c,s}^2\right)}{w_s^4} D*^4 \frac{1}{p} \left(\frac{v}{v_0 - v} \right)$$

The symbols and units used are listed in Appendix 1.

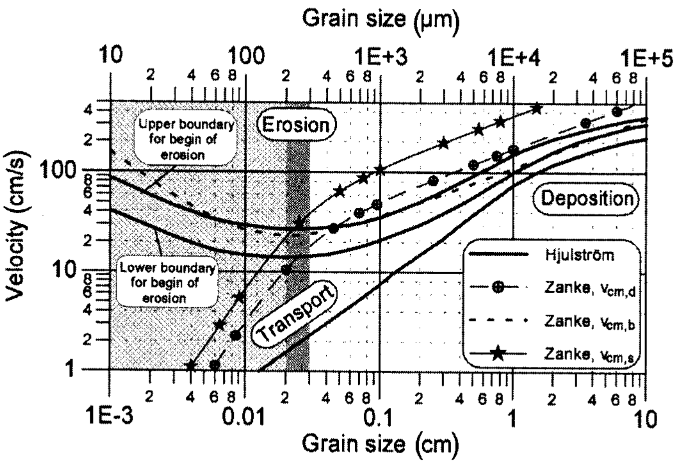

FIG. 3.—Critical velocities for initiating bed-load and suspension-load transport. The well-known Hjulström (1935) curve is given as reference. The critical velocities for beginning of deposition ($v_{cm,d}$), bed-load transport ($v_{cm,b}$), and suspension-load transport ($v_{cm,s}$) are approximated by polynomial equations given in Zanke (1977):

$$v_{cm,d} = 3.93\frac{12v}{d(2.7-2.3FF)}\left(\sqrt{1+\left\{0.21\left[\frac{\left(\frac{\rho_s-\rho_F}{\rho_F}\right)g}{v^2}\right]^{1/3}\right\}^3 (2.7-2.3FF)}-1\right)$$

$$v_{cm,b} = 2.8\left[\left(\frac{\rho_s-\rho_F}{\rho_F}\right)gd\right]^{0.5} + 14.7\frac{v}{d}c$$

where c = 1

$$v_{cm,s} = 8.4\frac{12v}{d(2.7-2.3FF)}\left(\sqrt{1+\left\{0.21\left[\frac{\left(\frac{\rho_s-\rho_F}{\rho_F}\right)g}{v^2}\right]^{1/3}\right\}^3 (2.7-2.3FF)}-1\right)$$

The symbols and units used are listed in Appendix 1.

the equations used is given in Haupt (1995), Haupt et al. (1997), and Seidov and Haupt (1997).

NUMERICAL EXPERIMENTS AND RESULTS

Ocean Circulation

In our study, we model the sediment accumulation process during the sequence of glacial and interglacial stages from the onset of the northern hemisphere glaciation, 2.62 Ma, until the present. We have chosen two time slices as reference sedimentation patterns. The first slice is the Holocene/modern (HM) warm interglacial stage; the second slice is the cold last glacial maximum (LGM) (18,000 ^{14}C yr; 21,600 calendar yr BP).

The HM experiment is based on the present-day oceanic conditions and climate system. The model was initialized with the winter temperatures and salinities of Levitus (1982) and Dietrich (1969). Wind stress was taken from Hellerman and Rosenstein (1983). To get the typical winter ice cover in the northern North Atlantic, the original temperatures were replaced by −1.9°C below ice (Wadhams, 1986). Additionally, the wind stress was set to zero when water was frozen. With these upper boundary conditions the OGCM shows the major currents around Iceland and in the Norwegian-Greenland Seas: the West Greenland Current, the East Greenland Current, the outflow through the Denmark Strait, the Irminger Current, the North Atlantic Current, the Norwegian Current parallel to the Norwegian Coastal Current, which enters the Barents Sea, and the West Svalbard Current, or the Transpolar Drift (Haupt et al., 1994, 1995, 1997). Bottom currents also are represented. South of Iceland these bottom currents match with the generalized circulation of bottom water given for the North Atlantic by McCave and Tucholke (1986). The model produces the Denmark Strait overflow water, the Iceland-Scotland overflow water, and the Wyville-Thomson Ridge overflow.

The LGM experiment shows, in contrast to the HM experiment, a southward shift of sea ice cover. The wind forcing was computed for the glacial summer at Max-Planck-Institute in Hamburg using the T42 atmospheric circulation model (Lautenschlager, 1991; Lautenschlager and Herterich, 1991). To include the glacial sea level fall, the overall depth was reduced by 100 m (Fairbanks, 1989; Bard et al., 1990; Seibold, 1993; Peltier, 1994). Shelf glaciation (Laurentide and European ice sheets) was imitated by a cutoff of all regions shallower than 200 m. This procedure cuts off the North Sea and the Barents Sea except the Bear Island Trough. Additionally, the cross-sectional areas of the straits around Greenland, Iceland, and Scotland are reduced. Based on the Levitus's (1982) reconstructions, sea surface salinities were modified in the northern part of the model area from reconstructions of Schulz (1994) and Sarnthein et al. (1994, 1995). At the southern part of the model area, the Levitus data set was updated by data from Duplessy et al. (1991). A detailed description of these data is given in Seidov et al. (1994). The CLIMAP (1981) summer reconstruction was used to include thermal forcing and ice cover. These LGM sea surface conditions lead to dramatic changes in ocean circulation in the Norwegian-Greenland Seas (Haupt et al., 1994; Haupt, 1995). The subtropical and subpolar gyres are reduced, and the Gulf Stream and the Labrador Current are weaker than in the HM experiment (Haupt et al., 1994). In the southern part of the Norwegian-Greenland Seas, the cyclonal gyre is intensified and strengthened by temperatures around the freezing point and by high salinity values (Haupt, 1995). The bottom currents south of the Greenland-Iceland-Scotland Ridge are still westward directed, but they are somewhat shifted and intensified.

Sediment Accumulation Patterns

The first glacial/interglacial experiments (scenario 1, consisting of HM1 and LGM1) with SEDLOB were initialized with the same sediment properties [sediment sources and sinking velocity of 0.05 cm/s = 43.2 m/d; i. e. <20 equalized sphere diameter (Shanks and Trent, 1980)]. As a sediment source we prescribed only a small flux of about 1.0×10^{-13} g/cm^2/s (0.0864 mg/m^2/d) caused by the eolian sediment (Miller et al., 1977; Honjo, 1990). The magnitude of the critical velocities for initiation of bed-load and suspension-load transport are reduced to 0.05 cm/s. In control runs we have found that it is necessary to simulate realistic transports in the bottom layer in the deeper ocean basins (Haupt et al., 1995; Seidov and Haupt, 1997). Previously published critical velocities (e.g., Hjulström, 1935; Zanke, 1978) are more representative for shallow marginal regions than for deep-sea regions. The modeled velocities are mean values and do not show, for example, tidal fluctuations, which also influence erosion and deposition, especially in coastal and shelf areas. In comparison to long-term mean currents from moored current-meter measurements in the East Greenland Current, our velocities are a factor of two to three too low (Fahrbach et al., 1995), which also is the case in other model results of the Norwegian-Greenland Seas (Legutke, 1989; Fahrbach et al., 1995). Further investigations are required to explain this discrepancy.

With all of these adjustments and constraints we were still able to reconstruct most known large sediment drifts, such as the drift south of the Greenland-Scotland Ridge, for both the HM and the LGM. In both experiments [HM1 (Figure 4A) and LGM1 (Figure 4B)] the resulting sediment patterns are predominantly along a northeast-southwest axis. In the LGM experiment (Figure 4B) the sediment accumulation structures are more pronounced. In comparison to the HM experiment (Figure 4A) with smoother sedimentation patterns, the maximum sedimentation rate increases from 5 cm/k.y. to up to 7 cm/k.y. Due to the different circulation patterns, the sedimentation patterns are noticeably different; however, in both experiments the model indicates high-accumulation areas in the same regions. These areas fit the Gloria Drift, Eirik Drift, Snorri Drift, Gadar Drift, Bjorn Drift, Hatton Drift, and the Feni Drift (McCave and Tucholke, 1986; Haupt et al., 1994; Haupt, 1995).

In a second set of experiments (scenario 2, consisting of HM2 and LGM1) we added to the modern experiment HM1 lateral sediment sources from rivers and coastal melting icebergs (Haupt, 1995; Haupt et al., 1997), but the glacial experiment remained unchanged; furthermore, we reduced the magnitudes of the critical velocities for bed-load and suspension-load transport to 0.002 cm/s and 0.02 cm/s, respectively. With these altered initial conditions the model was capable of eroding sediment when the critical velocities were weaker than the velocities predicted by the OGCM. With this justification, one can improve simulation of the observed sediment transport and erosion patterns, even though it produces more patchy sediment structures; nevertheless, the areas with higher sedimentation rates still fit the well-known sediment drifts (Figure 5).

Stratigraphic Control

North Atlantic site DSDP 607 (Raymo et al., 1989; Ruddiman et al., 1989), following the oxygen isotope time scale of Shackleton et al. (1990), was used for stratigraphic calibration of glacial and interglacial stages. From the astronomically tuned and globally correlated oxygen isotope record (cf. Tiedemann et al., 1994), stages 1–104 close to the Matuyama/Gauss magnetic boundary were used, covering the last 2.62 m.y. Cold and warm periods were distinguished based on the oxygen isotope curve. A continuous time sequence of 33 cold and 34 warm periods was elaborated, taking into account shifts in the time-dependent mean of oxygen isotope values (Mudelsee, 1995; Mudelsee and Stattegger, 1997) and a minimum duration of 15,000 yr per period to contribute noticeably to the buildup of the sediment column (see Table 1). This

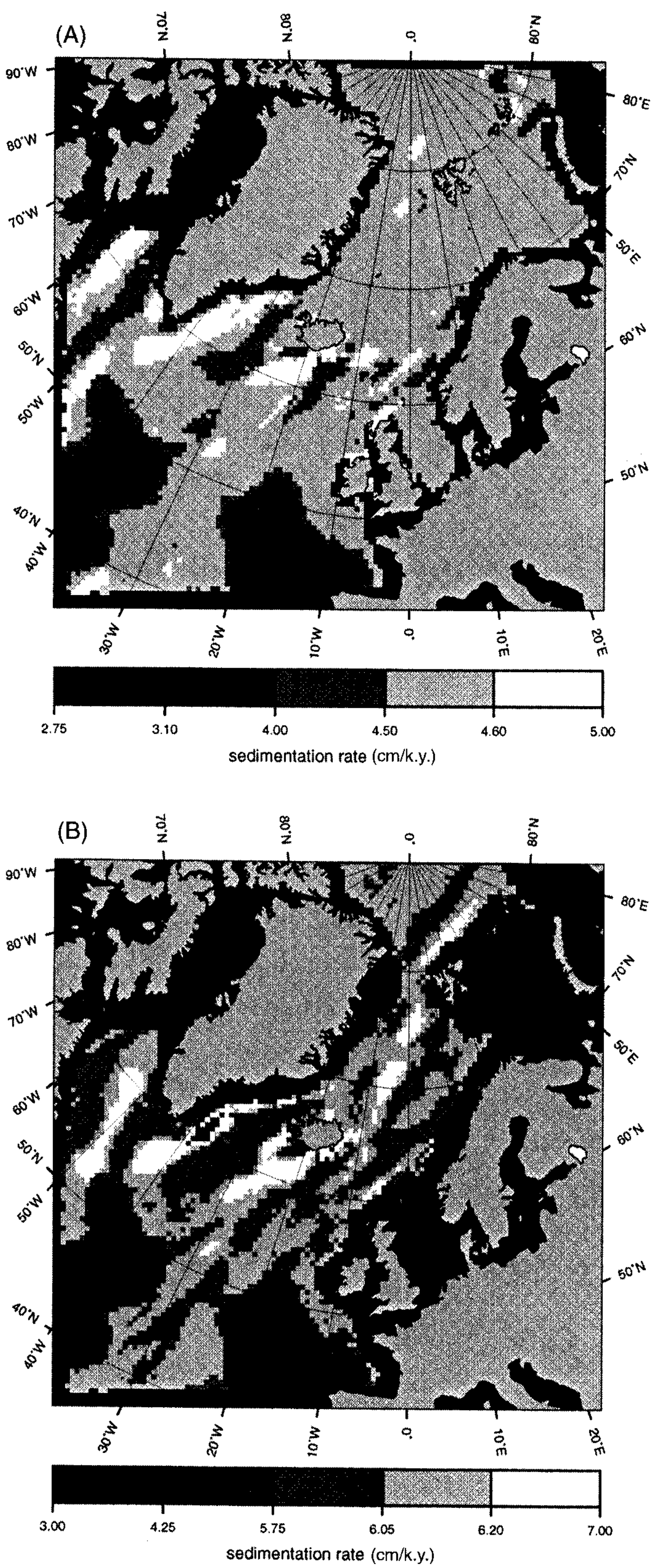

FIG. 4.—(A) Present-day and (B) last glacial maximum sedimentation rate (cm/1000 yr). Only the eolian sediment input from the atmosphere (1×10^{-13} g/cm^2/s ≈ 0.0864 mg/cm^2/d) is considered (Miller et al., 1977; Honjo, 1990). The critical velocities for starting of bed load and for beginning of suspension load are set to 0.05 cm/s.

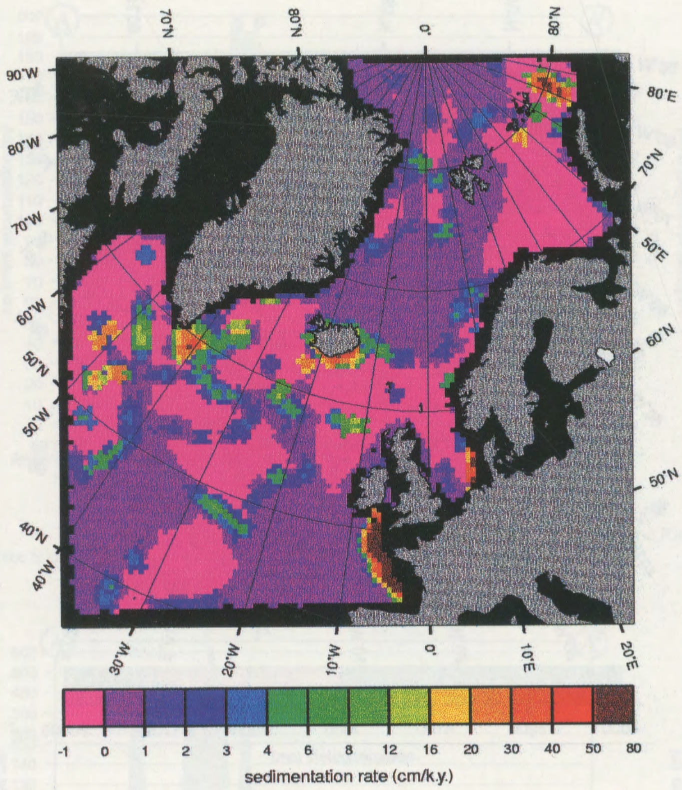

FIG. 5.—Present-day sedimentation rate (cm/1000 yr). In comparison to experiment HM1 (Figure 4A), additional lateral sediment sources from rivers and coastal melting icebergs are applied (Haupt, 1995; Haupt et al., 1997); furthermore, the critical velocities for starting of bed load and for beginning of suspension load are set to 0.002 cm/s and 0.02 cm/s, respectively, to initiate higher transports.

TABLE 1. CONTINUOUS TIME SEQUENCE OF 33 COLD AND 34 WARM PERIODS COVERING THE LAST 2.62 M.Y.*

Climatic Period	Age (k.y.)	Duration (k.y.)	Climatic Period	Age (k.y.)	Duration (k.y.)
Warm	0–16	16	Warm	1420–1445	25
Cold	16–113	97	Cold	1445–1468	23
Warm	113–143	30	Warm	1468–1483	15
Cold	143–194	51	Cold	1483–1518	35
Warm	194–223	29	Warm	1518–1538	20
Cold	223–294	71	Cold	1538–1575	37
Warm	294 –327	33	Warm	1575–1624	49
Cold	327–374	47	Cold	1624–1655	31
Warm	374–421	47	Warm	1655–1679	24
Cold	421–477	56	Cold	1679–1695	16
Warm	477–497	20	Warm	1695–1729	34
Cold	497–516	19	Cold	1729–1754	25
Warm	516–589	73	Warm	1754–1775	21
Cold	589–662	73	Cold	1775–1801	26
Warm	662–697	35	Warm	1801–1917	116
Cold	697–790	93	Cold	1917–1960	43
Warm	790–817	27	Warm	1960–1985	25
Cold	817–853	36	Cold	1985–2006	21
Warm	853–950	97	Warm	2006–2022	16
Cold	950–983	33	Cold	2022–2037	15
Warm	983–1052	69	Warm	2037–2092	55
Cold	1052–1072	20	Cold	2092–2131	39
Warm	1072–1128	56	Warm	2131–2166	35
Cold	1128–1159	31	Cold	2166–2191	25
Warm	1159–1185	26	Warm	2191–2278	87
Cold	1185–1242	57	Cold	2278–2296	18
Warm	1242–1259	17	Warm	2296–2424	128
Cold	1259–1290	31	Cold	2424–2454	30
Warm	1290–1319	29	Warm	2454–2471	17
Cold	1319–1336	17	Cold	2471–2525	54
Warm	1336–1359	23	Warm	2525–2576	51
Cold	1359–1377	18	Cold	2576–2595	19
Warm	1377–1396	19	Warm	2595–2620	25
Cold	1396–1420	24			

*Filtered out from the North Atlantic site DSDP 607 (Ruddiman et al., 1989; Raymo et al., 1989). On the base of the oxygen isotope curve (running mean), Mudelsee and Stattegger (1997) took only periods with a minimum duration of 15000 yr, which will contribute noticeably in the buildup of the sediment column.

glacial/interglacial sequence provides the time frame for the basin-fill stacking in succeeding cold/warm sedimentation patterns.

Stratigraphic Simulation

Time integration and stacking of glacial and interglacial sedimentation patterns results in the climatically forced basin fill of the northern North Atlantic for the last 2.62 m.y. Scenario 1 (Figure 6) uses the sedimentation pattern shown in Figure 4A for the interglacial state and that shown in Figure 4B for the glacial state. Sediment input is provided only from the sea surface, and erosion is absent due to high critical velocities. Scenario 2 (Figure 7) takes into account fluvial input during interglacial periods; slight areal erosion also takes place regionally due to lower critical velocities. This scenario combines the sedimentation patterns of Figure 5 (interglacial) and Figure 4B (glacial). The initial sediment height at the base 2.62 m.y. was set to zero. From there, we integrated linearly between glacial and interglacial stages to the present.

We are conscious of the fact that using only two climatic stages (interglacial = warm = modern state; glacial = cold = LGM) leads to an oversimplified stratigraphic stacking pattern. Many intermittent periods of "cold" climate over the past 2.6 m.y. are significantly different from the LGM; nevertheless, the modern and the LGM climates are extreme scenarios characterized by maximal differences in oceanic circulation and sedimentation.

To elucidate the stratigraphic architecture of this glacial/interglacial basin fill, we created two characteristic cross sections. The first 3635-km-long stratigraphic cross section AA′ follows the Greenland-Iceland-Faeroer-Scotland Ridge and continues into the Labrador Sea, and is composed of northwest-southeast and west-east segments. The second cross section BB′ extends over 4689 km in a southwest-northeast direction from the Mid-Atlantic Ridge to the Barents Sea continental margin (see Figure 6 for location). The endpoints A, A′, B, and B′ mark the glacial sea level coastline shelf border.

Scenario 1.—

Cross section AA′ (Figure 8A) contains the synthetic stratigraphy of the Greenland-Iceland-Faeroer-Scotland Ridge in Scenario 1. The rugged surface developed continuously during glacial and interglacial periods due to the morphologically driven ocean currents in the ridge area. This ocean circulation is responsible for similar lateral variations in sedimentation rates providing only surficial sediment input. Cumulative sediment thicknesses range between 110 and 250 m along the section, with the most prominent sedimentation peaks occurring around Iceland. Cross section BB′ (Figure 8B) shows a smooth architecture with a depression southeast of Iceland. The average height of the sediment fill amounts to approximately 160 m, about 20% more than that measured in ODP cores from this region.

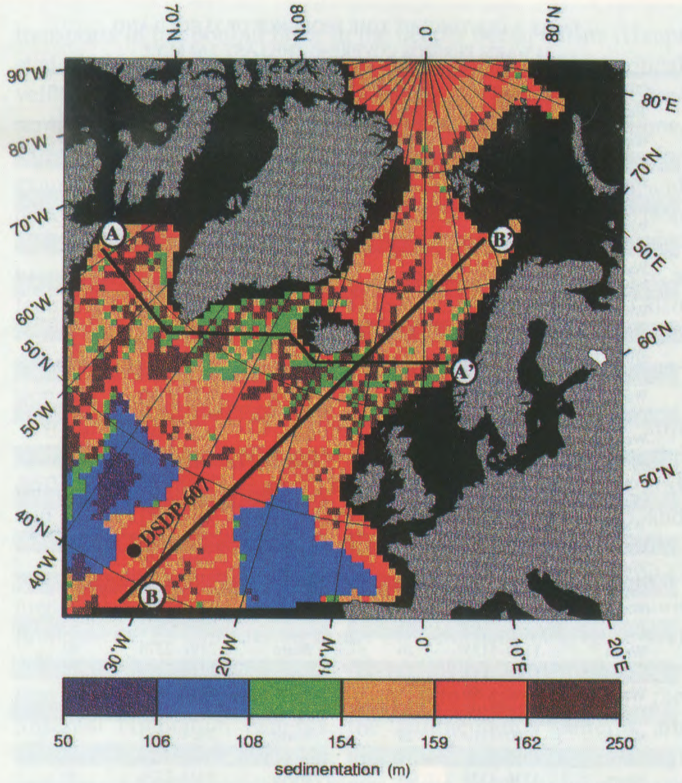

FIG. 6.—Time integration and stacking of glacial and interglacial sediment patterns for Scenario 1. This scenario uses the sedimentation pattern shown in Figure 4A for the interglacial state and that shown in Figure 4B for the glacial state. Additionally, the locations of cross sections AA′ and BB′ (see Figures 8 and 9) and the location of the North Atlantic site DSDP 607 are shown.

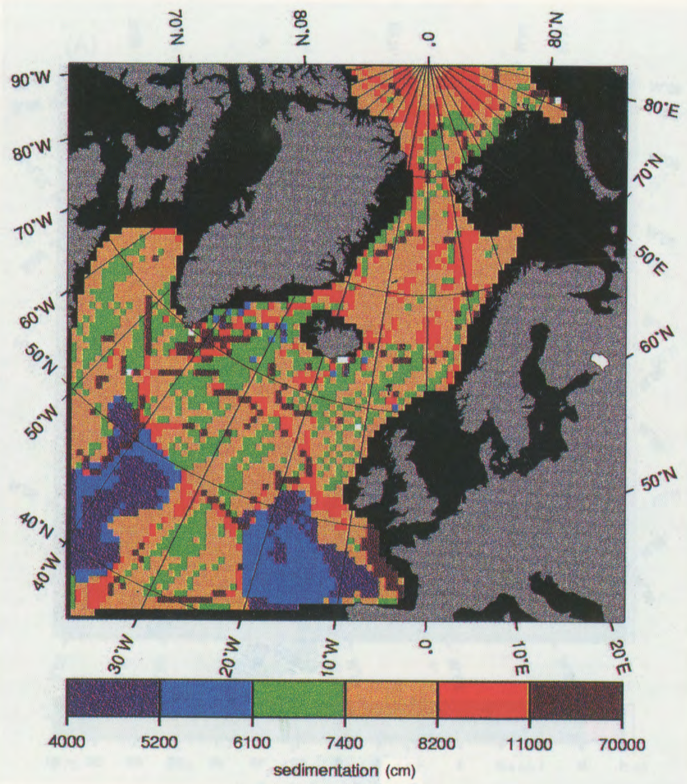

FIG. 7.—Time integration and stacking of glacial and interglacial sediment patterns for Scenario 2. This scenario uses the sedimentation pattern shown in Figure 5 for the interglacial state and that shown in Figure 4B for the glacial state.

Scenario 2.—

Cross section AA′ (Figure 9A) shows a rugged surface again. The stratigraphic column is built up to a large extent during glacial periods and slightly eroded during interglacials; therefore, sediment thicknesses are generally lower compared to Scenario 1. The sequence is interrupted by four interglacial high-sedimentation peaks southeast of Greenland. The synthetic stratigraphic section implies high sediment accumulation in certain areas of the Greenland-Iceland-Faeroer-Scotland Ridge building up the well-known large sediment drifts that are strongly affected by a remote source of fluvial sediment input. The interglacial sediment oscillations reach several hundreds of meters, allowing a maximum sedimentation rate of 30 cm/k.y., whereas the glacial oscillations are reduced by a factor of ten. Cross section BB′ (Figure 9B) exhibits a smoother sediment sequence accumulated during glacials, with some smaller peaks that developed during interglacials.

CONCLUSIONS

From our numerical experiments we conclude that stratigraphic sequences in an ocean basin can be simulated successfully if we are able to model initially the oceanic circulation and its sedimentary response for specific reference time slices. Integrating such scenarios over time spans provided by the general stratigraphic record of a basin enables us to model the three-dimensional basin fill and resulting synthetic stratigraphic sequences.

Because sediment accumulation in ocean basins is a response to ocean currents, a suitable stratigraphic modeling approach must take into account this strong dependence by coupling the processes of erosion, transport, and deposition of sediments to specific oceanic circulation patterns that refer to climatic conditions and basin morphology.

From the two scenarios presented to construct stratigraphic sequences in the northern North Atlantic it is evident that certain areas of the Greenland-Iceland-Faeroer-Scotland Ridge accumulate substantially more sediment than the rest of the basin. Especially during interglacial periods, existing high-sedimentation areas can be intensified by fluvial input, implying that sediment accumulation at these regions is initiated by bottom topography and ocean currents and increased by fluvial input.

Scenario 1 tends to overestimate sedimentation in general because of the lack of erosion and to underestimate sediment fluxes during interglacials because it neglects fluvial input. For Scenario 2, restrictions of the maximum sedimentation rate during interglacials have to be set to avoid unreasonably high local sediment accumulation over longer time spans. High-sedimentation areas fed by fluvial input are locally restricted, whereas low sedimentation rates prevail over large areas.

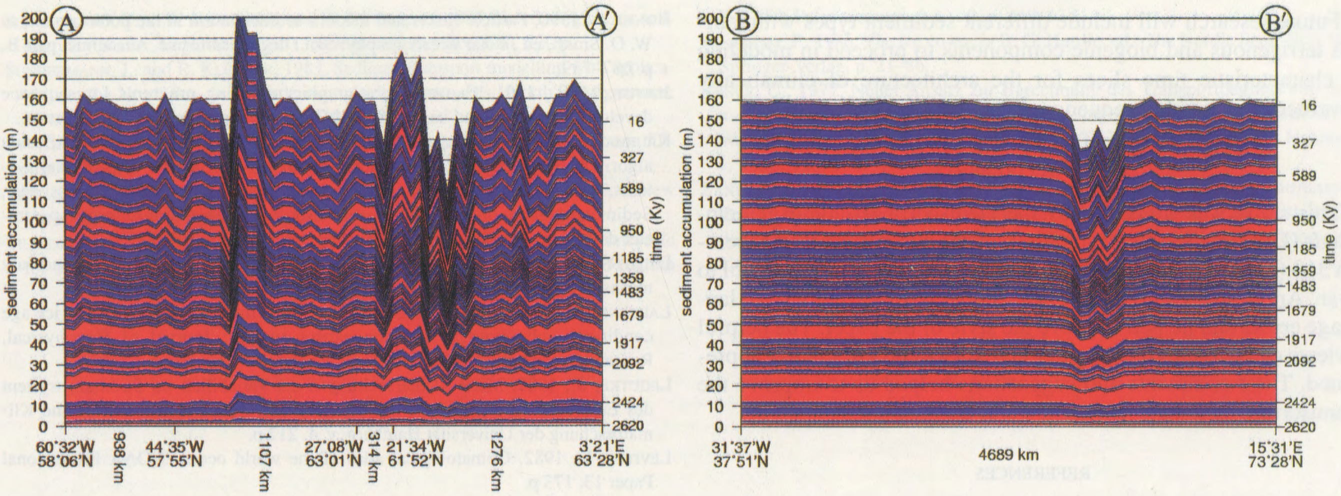

FIG. 8.—Synthetic stratigraphy (A) along the Greenland-Iceland-Faeroer-Scotland Ridge and (B) from the Mid-Atlantic Ridge to the border of the Barents Shelf in Scenario 1 (see text). The cross sections AA′ and BB′ are shown in Figure 6.

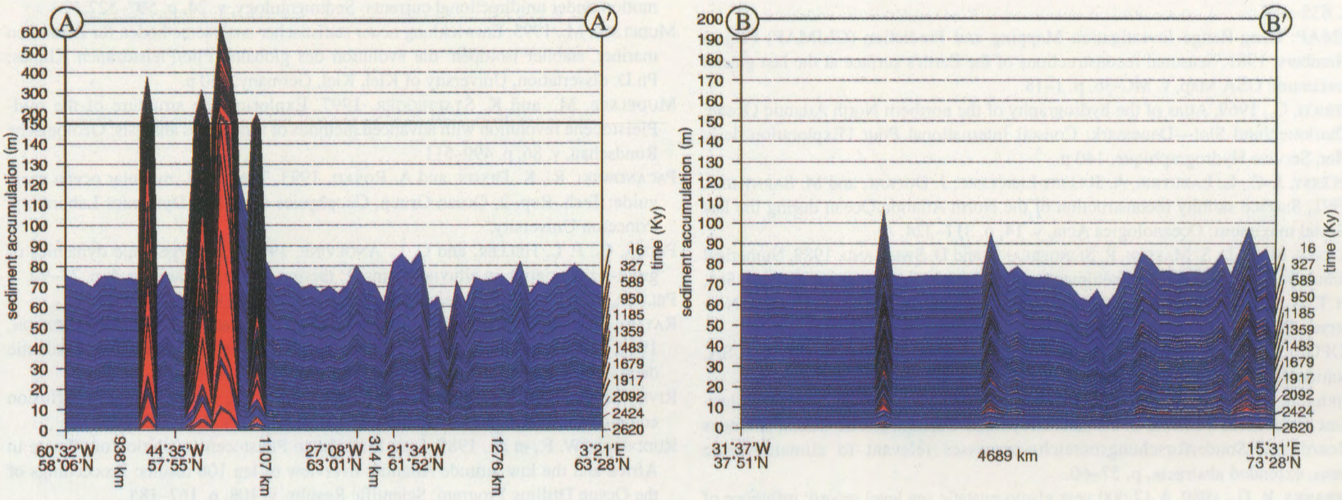

FIG. 9.—Synthetic stratigraphy (A) along the Greenland-Iceland-Faeroer-Scotland Ridge and (B) from the Mid-Atlantic Ridge to the border of the Barents shelf in Scenario 2 (see text). The cross sections AA′ and BB′ are shown in Figure 6.

APPENDIX 1

Symbol	Definition	Units
D	Grain size	cm
D^*	Sedimentological grain diameter $[(\rho' g/\nu^2)1/3]d$	–
FF	Form factor	–
G	Gravitational acceleration	g/cm/s^2
h_{sed}	Change of bottom topography due to erosion, transport, and deposition	cm
H	Water depth	cm
p	Pressure	g/cm/s
q_B, q_S	Bed-load and suspension-load transport, respectively	cm3/cm/s
$v_{cmvb}, v_{cms}, v_{cmd}$	Critical velocities for beginning of bed-load transport, suspension-load transport, and deposition, respectively	cm/s
u_{bop}, v_{bot}	Reduced zonal and meridional bottom velocity components	cm/s
$\vec{v}, \vec{v}_{bot}$	Three-dimensional and two-dimensional velocity vector	cm/s
w_S	Settling velocity	cm/s
ν	Kinematic viscosity of sea water	cm^2/s
ρ_F, ρ_S	Density of sea water and sediment	g/cm^3
ρ'	Relative density $[(\rho_S - \rho_F)/\rho_F]$	–

Future research will include different sediment types with various terrigenous and biogenic components to proceed in modeling of characteristic time slices for the architecture of climatically governed stratigraphic sequences.

ACKNOWLEDGMENTS

This study was supported by the Deutsche Forschungsgemeinschaft (DFG) within the framework of the Sonderforschungsbereich 313 (SFB 313 Project B4) at Kiel University. We are grateful to Avan Antia and Dan Seidov, who corrected our numerous language errors and helped improve the style of the paper. The helpful reviews of William W. Hay and Peter J. Fawcett are greatly appreciated. Their comments and suggestions helped us to improve the manuscript.

REFERENCES

BARD, E., B. HAMELIN, R. G. FAIRBANKS, and A. ZINDLER, 1990, Calibration of the ^{14}C timescale over the past 30,000 years using mass spectrometric U-Th ages from Barbados Corals: Nature, v. 345, p. 405–410.

CAO, S., and I. LERCHE, 1994, A quantitative model of dynamical sediment deposition and erosion in three dimensions: Computer and Geosiences, v. 20, no. 4, p. 635–663.

CLIMAP: Long-Range Investigation Mapping and Prediction (CLIMAP) Project Members, 1981, Seasonal reconstructions of the Earth's surface at the last glacial maximum: GSA Map, v. MC-36, p. 1–18.

DIETRICH, G., 1969, Atlas of the hydrography of the northern North Atlantic Ocean: Charlottenlund Slot—Danemark: Conseil International Pour l'Exploration de la Mer, Service Hydrographique, 140 p.

DUPLESSY, J.-C., L. LABEYRIE, A. JULLIET-LERCLERC, J. DUPRAT, and M. SARNTHEIN, 1991, Surface salinity reconstruction of the North Atlantic Ocean during the last glacial maximum: Oceanologica Acta, v. 14, p. 311–324.

ERICKSEN, M. C., D. S. MASSON, R. SLINGERLAND, and D. SWETLAND, 1989, Numerical simulation of circulation and sediment transport in the late Devonian Catskill Sea, *in* T. A. Cross, ed., Quantitative dynamic stratigraphy: Englewood Cliffs, New Jersey, Prentice-Hall, p. 293–305.

ETOPO5, 1986, Digital relief of the surface of the earth: Boulder, Colorado, USA, National Geophysical Data Center.

FAHRBACH, E., CH. HEINZE, G. ROHARD, and R. A. WOODGATE, 1995, Moored current meter measurements in the East Greenland Current: Arctic Ocean Sciences Board and Sonderforschungsbereich, processes relevant to climate/Nordic Seas, extended abstracts, p. 57–60.

FAIRBANKS, R. G., 1989, A 17,000 year glacio-eustatic sea level record: influence of glacial melting rates on the Younger Dryas event and deep-ocean circulation: Nature, v. 342, p. 637–642.

FLEMINGS, P. B., and J. P. GROTZINGER, 1996, STRATA: freeware for analyzing classic stratigraphic problems: GSA Today, v. 6, no. 12, p. 1–7.

HAUPT, B. J., 1995, Numerische modellierung der sedimentation im nördlichen Nordatlantik: Germany, University of Kiel, v. 54, 129 p.

HAUPT, B. J., and K. STATTEGGER, 1996, Data based modeling of the ocean-sediment system in large basins, *in* W. L. Watney, E. C. Rankey, E. K. Franseen, and R. H. Goldtstein, eds., Numerical experiments in stratigraphy, an international workshop: Lawrence, Kansas, University of Kansas, 164 p.

HAUPT, B. J., C. SCHÄFER-NETH, and K. STATTEGGER, 1994, Modelling sediment drifts; a coupled oceanic circulation-sedimentation model of the northern North Atlantic: Paleoceanography, v. 9, no. 6, p. 897–916.

HAUPT, B. J., C. SCHÄFER-NETH, and K. STATTEGGER, 1995, 3-D numerical modelling of late Quaternary paleoceanography and sedimentation in the northern North Atlantic: Geologische Rundschau, v. 84, p. 137–150.

HAUPT, B. J., D. SEIDOV, and K. STATTEGGER, 1997, SEDLOB and PATLOB: two numerical tools for modeling climatically forced sediment and water volumes transport in large ocean basins, *in* J. Harff, K. Stattegger and W. Leurke, eds., Computerized modeling of sedimentary systems: New York, Springer-Verlag, p. 33.

HELLERMAN, S., and M. ROSENSTEIN, 1983, Normal monthly wind stress over the world ocean with error estimates: Journal of Physical Oceanography, v. 13, p. 1093–1104.

HJULSTRÖM, F., 1935, Studies of the morphological activity of rivers as illustrated by the river Fyris: Bulletin of the Geological Institution of the University of Upsala, Upsala, 221–527.

HONJO, S., 1990, Particle fluxes and modern sedimentation in the polar oceans, *in* W. O. Smith, ed., Polar oceanography: San Diego, California, Academic, part B, p. 687–739.

JERVEY, M. T., 1991, GEOMOD: stratigraphic modeling programs for sequence development in foreland basins: SEPM Computer Contribution 2, 3 diskettes.

KAUFMAN, P., J. P. Grotzinger, and D. S. McCormick, 1991, Depth-dependent diffusion algorithm for simulation of sedimentation in shallow marine depositional systems, *in* E. K. Franseen, W. L. Watney, C. G. St. C. Kendall, and W. Ross, eds., Sedimentary modeling: computer simulation and methods for improved parameter definition: Kansas Geological Survey Bulletin. 233, p. 489–508.

LAUTENSCHLAGER, M., 1991, Simulation of ice age atmosphere—January and July means: Geologische Rundschau, v. 80, no. 3, p. 513–534.

LAUTENSCHLAGER, M., and K. HERTERICH, 1991, Atmospheric response to ice age conditions—climatology near the earth's surface: Journal of Geophysical. Research, v. 95, p. 22,547–22,557.

LEGUTKE, S., 1989, Modell-Untersuchungen zur variabilität im Strömungssystem des Europäischen Nordmeers: Berichte aus dem Zentrum für Meeres- und Klimaforschung der Universität Hamburg, v. 4, 212 p.

LEVITUS, S., 1982, Climatological atlas of the world ocean: NOAA Professional Paper 13, 173 p.

MCCAVE, I. N., and B. E. TUCHOLKE, 1986, Deep current controlled sedimentation in the western North Atlantic, *in* P. R. Vogt and B. E. Tucholke, eds., The geology of North America; the western North Atlantic region: Boulder, Colorado, Geological Society of America, v. M, p. 451–468.

MILLER, M. C., I. N. MCCAVE, and P. D. KOMAR, 1977, Threshold of sediment motion under unidirectional currents: Sedimentology, v. 24, p. 507–527.

MUDELSEE, M., 1995, Entwicklung neuer statistischer analysemethoden für Zeitreihen mariner, stabiler isotopen: die evolution des globalen Plio/Pleistozänen Klimas: Ph.D. dissertation, University of Kiel, Kiel, Germany, 150 p.

MUDELSEE, M., and K. STATTEGGER, 1997, Exploring the structure of the mid-Pleistocene revolution with advanced methods of time series analysis: Geologische Rundschau, v. 86, p. 499–511.

PACANOWSKI, R., K. DIXON, and A. ROSATI, 1993, The GFDL modular ocean users guide: Tech. Rep. 2, Ocean Group, Geophysics and Fluid Dynamics Laboratory, Princeton University,

PAOLA, C., P. L. HELLER, and C. L. ANGEVINE, 1992, The large scale dynamics of grain-size variation in alluvial basins, 1: theory: Basin Research, v. 4, p. 73–90.

PELTIER, W. R., 1994, Ice age paleotopography: Science, v. 265, p. 195–201.

RAYMO, M. E., W. F. RUDDIMAN, J. BACKMAN, B. M. CLEMENT, and D. G. MARTINSON, 1989, Late Pliocene variation in northern hemisphere ice-sheets and North Atlantic deep water circulation: Paleoceanography, v. 4, p. 413–446.

RIVENAES, J. C., 1992, Application of a dual lithology, depth-dependent diffusion equation in stratigraphic simulation: Basin Research, v. 4, p. 133–146.

RUDDIMAN, W. F., et al., 1989, Late Miocene to Pleistocene evolution of climate in Africa and the low latitude Atlantic: overview of leg 108 results: Proceedings of the Ocean Drilling Program, Scientific Results, v. 108, p. 167–185.

SARNTHEIN, M., K. WINN, S. J. A. JUNG, J. C. DUPLESSY, L. LABEYRIE, H. ERLENKEUSER, and G. GANSSEN, 1994, Changes in east Atlantic deepwater circulation over the last 30,000 years—eight time slice reconstructions: Paleoceanography, v. 9, p. 209–267.

SARNTHEIN, M., et al., 1995, Variations in Atlantic Ocean paleoceanography, 50°–80°N: a time slice record of the last 30,000 years: Paleoceanography, v. 10, p. 1063–1094.

SCHÄFER-NETH, C., 1994, Modellierung der Paleoozenaographie des nördlichen Nordatlantiks zur letzten Maximalvereisung: Germany, University of Kiel, v. 51, 106 p.

SCHULZ, H., 1994, Meeresoberflächentemperaturen im frühen Holozän 10,000 Jahre vor heute: Ph.D. dissertation, University of Kiel, Kiel, Germany, 250 p.

SEIBOLD, E., 1993, Das Meer—Ein Schlüssel zur Geologie: Naturwissenschaftliche Rundschau, v. 46, no. 2, p. 43–50.

SEIDOV, D., and B. J. HAUPT, 1997, Simulated ocean circulation and sediment transport in the North Atlantic during the last glacial maximum and today: Paleoceanography, v. 12, no. 2, p. 281–305.

SEIDOV, D., M. SARNTHEIN, K. STATTEGGER, R. PRIEN, and M. WEINELT, 1994, Toward a better understanding of the meltwater event near 13.6 k.y. BP—a numerical modeling approach: Journal of Geophysical Research, v. 101, no. C7, p. 16,305–16,332.

SHACKLETON, N. J., A. BERGER, and W. R. PELTIER, 1990, An alternative astronomical calibration of the lower Pleistocene time scale based on ODP site 677: Transactions of the Royal Society, v. 81, p. 251–261.

SHANKS, A. L., and J. D. Trent, 1980, Marine snow: sinking rates and potential role in vertical flux: Deep Sea Research, part A, v. 27, p. 137–143.

SLINGERLAND, R., J. W. HARBAUGH, and K. P. FURLONG, 1994, Simulating clastic sedimentary basins: Englewood Cliffs, New Jersey, Prentice-Hall, 220 p.

SÜNDERMANN, J., and R. KLÖCKER, 1983, Sediment transport modelling with applications to the North Sea, *in* J. Sündermann and W. Lenz, eds., North Sea dynamics: New York, Springer-Verlag, p. 453–471.

SYVITSKI, J. P. M., and S. DAUGHNEY, 1992, DELTA2: delta progradation and basin filling: Computer and Geosciences, v. 18, no. 7, p. 839–897.

TETZLAFF, D. M., and J. W. HARBAUGH, 1989, Simulating clastic sedimentation: New York, Van Nostrand Reinhold, 202 p.

TIEDEMANN, R., M. SARNTHEIN, and N. J. SHACKLETON, 1994, Astronomic timescale for the Pliocene Atlantic $\delta^{18}O$ and dust flux records of Ocean Drilling Program Site 659: Paleoceanography, v. 9, p. 619–638.

WADHAMS, P., 1986, The ice cover, *in* B. G. Hurdle, ed., The Nordic Seas: New York, Springer-Verlag, p. 21–86.

ZANKE, U., 1977, Neuer Ansatz zur Berechnung des Transportbeginns von Sedimenten unter Strömungseinfluβ: Mitteilungen des Franzius-Instituts für Wasserbau und Küsteningenieurswesen der Technischen Universität Hannover, v. 46, p. 156–178.

ZANKE, U., 1978, Zusammenhänge zwischen Strömung und Sedimenttransport; Teil 1: Berechnung des Sedimenttransportes—allgemeiner Fall: Mitteilungen des Franzius-Instituts für Wasserbau und Küsteningenieurswesen der Technischen Universität Hannover, v. 47, p. 214–345.